EPJ Photovoltaics **5**, 55201 (2014)
www.epj-pv.org
DOI: 10.1051/epjpv/2013027

UV and IR laser induced ablation of Al_2O_3/SiN:H and a-Si:H/SiN:H

T. Schutz-Kuchly[1,a], A. Slaoui[1], J. Zelgowski[2], A. Bahouka[2], M. Pawlik[3], J.-P. Vilcot[3], E. Delbos[4], M. Bouttemy[5], and R. Cabal[6]

[1] Laboratoire des sciences de l'Ingénieur, de l'Informatique et de l'Imagerie (ICUBE) UMR 7357, UdS/CNRS, 23 rue du Loess, BP 20 CR, 67037 Strasbourg Cedex 2, France
[2] IREPA-Laser Pole API – Parc d'innovation, 67400 Strasbourg, France
[3] Institut d'Électronique, de Microélectronique et de Nanotechnologie (IEMN) UMR 8520, Université Lille 1 Sciences et Technologies, CS 60069, 59652 Villeneuve d'Ascq, France
[4] KMG Group, 45 avenue des États-Unis, 78035 Versailles, France
[5] Institut Lavoisier de Versailles UMR 8180, Université de Versailles-St-Quentin en Yvelines, 45 avenue des États-Unis, 78000 Versailles, France
[6] CEA-INES, 50 avenue du Lac Léman, 73375 Le Bourget du Lac, France

Received: 24 July 2013 / Received in final form: 9 October 2013 / Accepted: 18 October 2013
Published online: 22 January 2014

Abstract Experimental work on laser induced ablation of thin Al_2O_3(20 nm)/SiN:H (70 nm) and a-Si:H (20 nm)/SiN:H (70 nm) stacks acting, respectively, as p-type and n-type silicon surface passivation layers is reported. Results obtained using two different laser sources are compared. The stacks are efficiently removed using a femtosecond infra-red laser (1030 nm wavelength, 300 fs pulse duration) but the underlying silicon surface is highly damaged in a ripple-like pattern. This collateral effect is almost completely avoided using a nanosecond ultra-violet laser (248 nm wavelength, 50 ns pulse duration), however a-Si:H flakes and Al_2O_3 lace remain after ablation process.

1 Introduction

In today's photovoltaic (PV) industry, laser processing is mostly limited to edge isolation [1] for producing standard silicon solar cells. Owing to its versatility, cost-effectiveness and high throughput, laser processing is well adapted for the PV industry need. For instance, laser doping has entered into production since 2009 for the fabrication of selective emitter solar cells [2]. Next step would be the use of laser induced ablation of dielectrics towards the fabrication of selective emitter silicon solar cells by structuring narrow lines into the antireflective coating. This will lead to increase the short circuit current by reducing electrode shadowing loss.

Selective laser ablation is particularly interesting when it is combined to self aligned metallization technologies such as nickel (Ni) electro-less deposition [3] and copper (Cu) plating. This combination can be seen as an attractive alternative to the standard screen-printed metallization which becomes a bottleneck in the PV industry because its use of expensive silver. Moreover, since the Ni-Cu metallization implies lower thermal budget than conventional screen printing route, surface passivation using, for example, amorphous silicon will be feasible.

N-type bifacial solar cells [4] are passivated with an aluminum oxide/hydrogenated silicon nitride (Al_2O_3/SiN:H) stack on their front side (P-type emitter) and an SiN:H on their rear side (N-type). Laser ablation of one single SiN:H layer has been studied by several research groups and is now well understood [5–8]. The ablation of the Al_2O_3/SiN:H stack has already been studied by Jaffrennou et al. [9] and Jin et al. [10] using UV picosecond lasers. However, as Al_2O_3 shows no significant optical absorption coefficient for this wavelength range, its correct ablation seems to be problematic, whatever it is stacked or not with another material film.

So, we present hereby experimental results concerning laser induced ablation of two dielectric stacks that are used for the passivation of n-type bifacial solar cells; an Al_2O_3/SiN:H stack for the passivation of the boron front emitter and an a-Si:H/SiN:H stack for the passivation of the phosphorus rear back surface field (BSF). The results obtained using two different laser sources, in terms of laser

[a] e-mail: tschutzk@gmail.com

Table 1. UV and IR laser characteristics.

Laser	Wavelength (nm)	Pulse duration	Profile	Frequency
UV	248	50 ns	Flat-hat	1−10 Hz
IR	1030	300 fs	Gaussian	0−2 MHz

wavelength and pulse duration, are compared. The first laser source is in the infra-red (IR) domain with a pulse duration of 300 fs and the second laser source is in the ultra-violet (UV) domain with a pulse duration of 50 ns.

The impact of the laser ablations on the silicon wafer is characterized in terms of carrier lifetime mappings. Scanning electron microscope (SEM) observations are used to visualize the ablation quality and the surface damages.

2 Experimental details

2.1 Laser characteristics

The characteristics of the two laser sources that were used are given in Table 1.

The first one is a femtosecond IR laser (1030 nm) with pulse duration of 300 fs from AMPLITUDE Systems, the model is Tangerine®. Minimum achievable spot size is close to 40 μm and the repetition frequency can reach up to 2 MHz which is an interesting feature for industrial purposes.

The second laser source is a Lambda Physics COMPex 201 UV Krypton Fluorine (KrF) excimer laser. The pulse duration is 50 ns and the repetition frequency is low, about 10 H. The typical spot size is around 3×3 mm^2 and physical masks will be used in order to pattern the substrates.

2.2 Wafer processing and characterization tools

The samples used in this work are 5×5 cm^2 squares issued from 125 PSQ Czochralski (Cz) N-type silicon wafers. The base resistivity is ∼3 Ω cm and the thickness is ∼200 μm. The samples were either KOH/IPA texturized or KOH polished.

The a-Si:H and the SiN:H layers were deposited in an electron-cyclotron-resonance plasma enhanced chemical vapor deposition (ECR-PECVD) reactor from Roth and Rau company. The a-Si:H and SiN:H thickness is 20 nm and 70 nm, respectively.

The Al_2O_3 layer was deposited in a plasma assisted atomic layer deposition (PA-ALD) reactor (BeneqTFS 200); its thickness is 20 nm. A SiN:H layer was also deposited on top.

The SEM analyses were performed using a SEM-FEG (Scanning Electron Microscope enhanced by a Field Emission Gun) equipment (JSM 7001-F, JEOL). Lifetime mappings were performed with a Semilab WT-2000 in Micro-Wave-Photoconductance-Decay (μW-PCD) mode. XPS (X-ray Photoelectron Spectroscopy) (Thermo Electron K-Alpha spectrometer) analyses and local nano-Auger measurements (Jamp 9500F, JEOL) were carried out over the ablated areas of the Al_2O_3/SiN:H coated wafers. Optical characterizations were performed with a Horiba Jobin-Yvon ellipsometer.

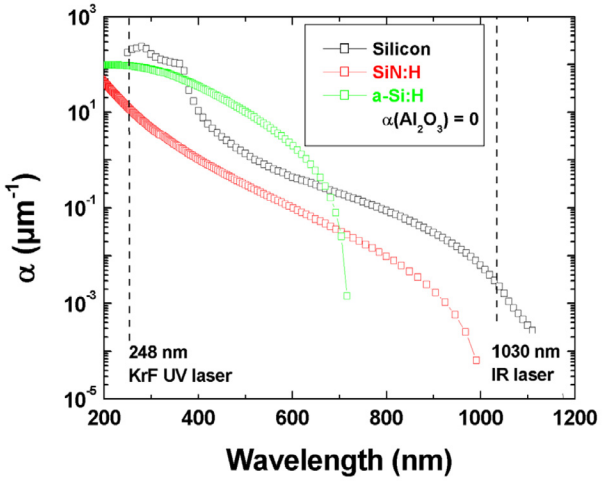

Fig. 1. Absorption coefficient (μm^{-1}) as a function of wavelength for silicon, SiN:H, a-Si:H and Al_2O_3.

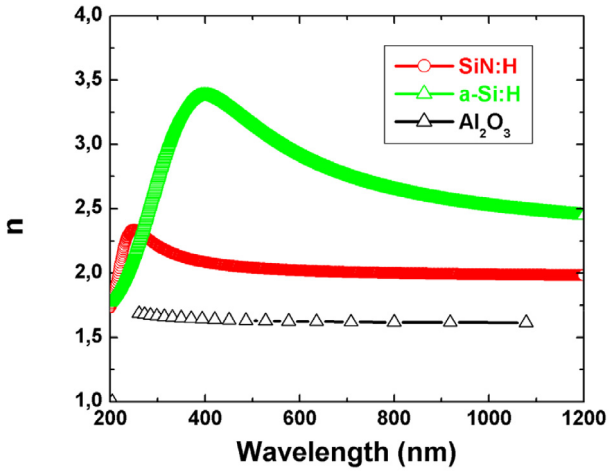

Fig. 2. Refractive index as a function of wavelength for SiN:H, a-Si:H and Al_2O_3.

3 Results and discussions

The optical properties of the different materials were firstly measured versus the wavelength. Absorption coefficient and refractive index are shown in Figures 1 and 2, respectively.

In the IR wavelength range of interest, the absorption coefficient of a-Si:H and SiN:H is negligible compared to silicon. In the UV wavelength range, the absorption coefficient of a-Si:H is similar to the one of silicon. Concerning Al_2O_3, the absorption coefficient remains almost 0, or in any case immeasurable, whatever the wavelength range is.

Table 2. Thermodynamic properties [11].

Name	c-Si	a-Si	Si_3N_4	Al_2O_3
T_m (°C)	1414	∼1200	1877	2072
T_b (°C)	3217	3217	N.A.	2977
k_{th} (W/(m °C))	150	<5	25	18

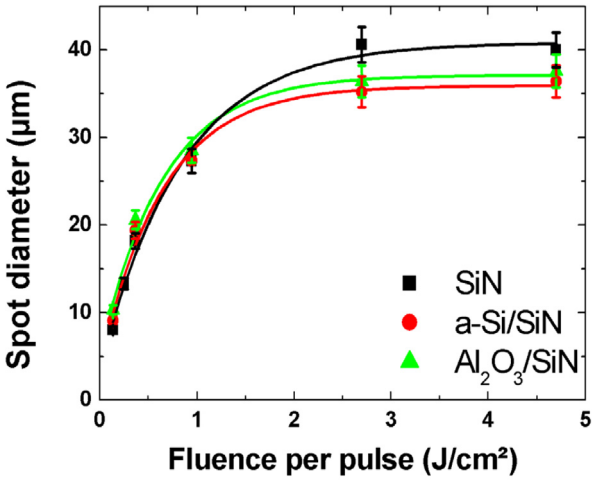

Fig. 3. Diameter of ablated spot versus fluence for SiN, a-Si:H/SiN:H, Al_2O_3/SiN:H materials.

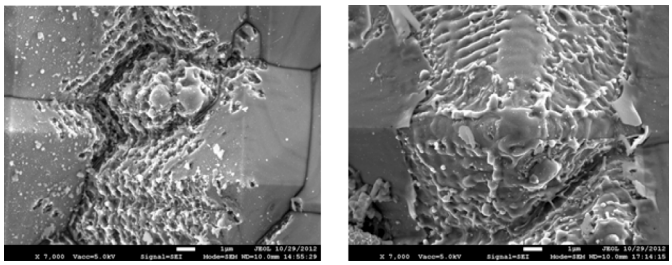

Fig. 4. SEM micrographs of ablated areas using the IR laser for a randomly texturized wafer covered with Al_2O_3/SiN:H. Left: Fluence close to ablation threshold. Right: High fluence value.

When performing ablation experiments, the thermodynamic properties of each material have to be kept in mind. Table 2 shows the melting temperature (T_m), the boiling temperature (T_b) and the thermal expansion coefficient (k_{th}) for silicon, Si_3N_4, a-Si, and Al_2O_3.

3.1 Ablation results using femtosecond IR laser

Based on optical microscope observations, Figure 3 shows the size of the ablated area as a function of the fluence value for three different layers: SiN:H, a-Si:H/SiN:H stack and Al_2O_3/SiN:H stack. The ablation threshold occurs at 0.14 J/cm^2 in any case. The ablated spot diameter reaches a plateau of ∼40 μm, for pulse energy densities greater than 2 J/cm^2.

Whatever it concerns an Al_2O_3/SiN:H (Fig. 4) or an a-Si:H/SiN:H (Fig. 5) stack deposited on a KOH texturized silicon surface, a ripple-like pattern can be observed

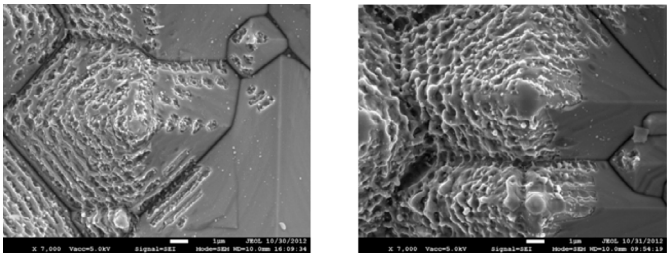

Fig. 5. SEM micrographs of ablated areas using the IR laser for a randomly texturized wafer covered with a-Si:H/SiN:H. Left: Fluence close to ablation threshold. Right: High fluence value.

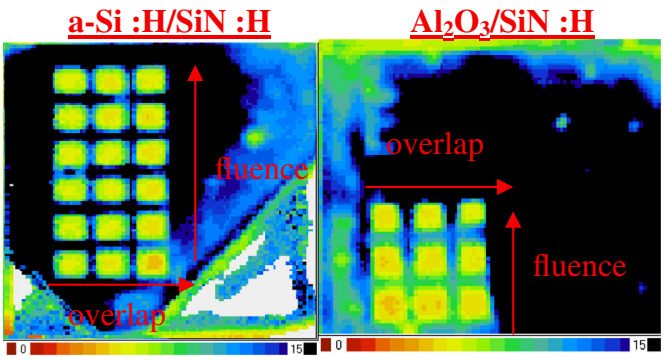

Fig. 6. Lifetime (μ s) mappings of re-passivated wafers. The areas irradiated by IR laser are 5×5 mm^2. Left: a-Si:H/SiN:H coated wafer. Right: Al_2O_3/SiN:H coated wafer.

over the ablated areas whatever the energy density is. This ripple-like pattern is caused by a modulated intensity pattern on the sidewalls of pyramids that is created by interference patterns during laser irradiation [12].

Based on the respective material absorption coefficients given in Figure 1, it can be seen that IR wavelength is mainly absorbed into the silicon substrate since a-Si:H, SiN:H and Al_2O_3 layers are transparent or quasi-transparent at 1030 nm. From the SEM observations (Figs. 4 and 5), we can speculate that the ripples are the resulting pattern of melted/re-crystallized silicon. As it seems that all the dielectric layers have been efficiently removed, it is reasonable to state that the difference in thermal expansion coefficient of silicon and of dielectric materials (see Tab. 2) was high enough for peeling the dielectric layers off.

In order to evaluate the substrate damages, lifetime mappings using μ W-PCD were performed (Fig. 6). Before performing these mappings, the wafers were HF dipped until the complete removal of Al_2O_3/SiN:H or a-Si:H/SiN:H stacks, and then re-passivated on both sides with a SiN:H film.

Figure 6 clearly shows that lifetime is degraded at the ablated areas. The decrease in lifetime is approximately the same when IR ablations are done on a-Si:H/SiN:H or Al_2O_3/SiN:H stack. Small variation of the lifetime value is observed on the ablated areas when the beam overlapping is increased. Same observation can be made when the fluence value is increased.

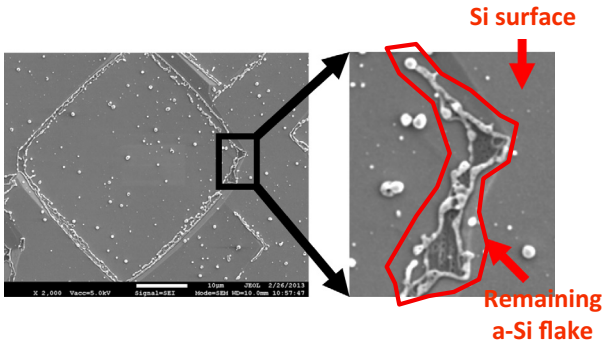

Fig. 7. SEM micrograph of an ablated area using UV laser on KOH polished wafer covered with a-Si:H/SiN:H film. Optimal fluence condition.

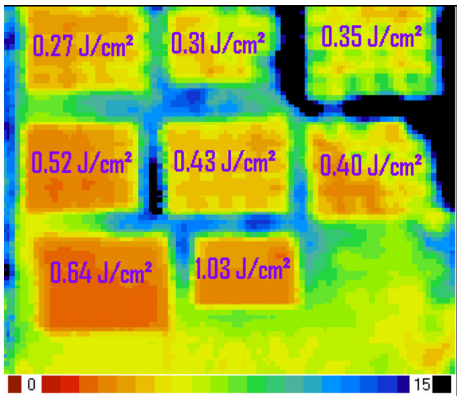

Fig. 8. Lifetime (μs) mapping of re-passivated a-Si:H/SiN:H wafer irradiated by UV laser.

3.2 Ablation results with nanosecond UV laser

3.2.1 a-Si:H/SiN:H stack

Same ablation experiments were done by using a KrF excimer laser. Ablation fluences were varied from ~0.3 J/cm^2 to 1.0 J/cm^2. Figure 7 shows a SEM picture of an ablated a-Si:H/SiN:H stack on a KOH-polished surface using an optimal fluence value. It can be seen that a-Si:H flakes are still present on the border of the truncated pyramids. It seems that a-Si:H material was melted and re-crystallized thus forming randomly distributed balls on the ablated surface.

As observed in the SEM micrograph, as no SiN:H remains and as the silicon wafer surface stays intact, we can reasonably state that the laser beam was absorbed in the a-Si:H/SiN:H stack and silicon wafer extreme surface. The increase in temperature due to the laser beam absorption induced the melting of the a-Si:H layer. The temperature increase was high enough to induce decomposition of the SiN:H layer [7].

Figure 8 shows the lifetime mapping of a re-passivated wafer that was a-Si:H/SiN:H coated. An expected decrease in lifetime is observed when the laser fluence increases. The increase between 0.31 J/cm^2 and 0.43 J/cm^2 (right top corner) is due to a local better wafer lifetime and not to less ablation damages.

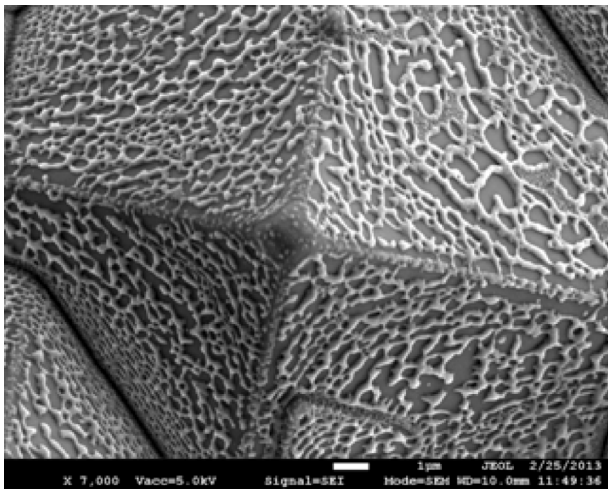

Fig. 9. SEM micrograph of an ablated area using UV laser on KOH textured wafer covered with Al_2O_3/SiN:H. Optimal fluence condition.

Table 3. XPS measurement results of the silicon surface after UV laser ablation of the Al_2O_3/SiN:H stack.

SiN	SiO_x	Metallic Si	Al_2O_3	Metallic C	CO
8.2%	58%	17.2%	2.5%	11.9%	4.2%

Table 4. Nano-Auger results after UV laser ablation of AL_2O_3/SiN:H stack.

C	O	Si	N	Al
11.3%	34.3%	32.8%	17.7%	3.9%

3.2.2 Al_2O_3/SiN:H stack

Figure 9 shows a SEM micrograph of the remaining Al_2O_3 material after ablation of an Al_2O_3/SiN:H stack deposited on a KOH textured silicon wafer. Al_2O_3 has been melted/re-crystallized resulting in a "lace" over the silicon surface. As for the a-Si:H/SiN:H case above reported, the heating during laser ablation induces the decomposition of SiN:H. As Al_2O_3 is transparent to the UV wavelength, its melting is induced by the heating of the silicon surface. As it can be seen on the pyramid tip (Fig. 9), the extreme silicon surface was melted as well.

The presence of the silicon surface in between the voids of the Al_2O_3 lace has been confirmed by XPS analysis, this is shown in Table 3. Local nano-Auger measurements show that this silicon surface has been doped with Al atoms from the Al_2O_3 layer (Tab. 4).

Figure 10 shows that lifetime is degraded on the ablated areas when the fluence is increased. It means that the silicon extreme surface is progressively damaged with increasing fluence value.

4 Conclusion

IR femtosecond and UV nanosecond lasers were investigated for the ablation of thin Al_2O_3 (20 nm)/SiN:H

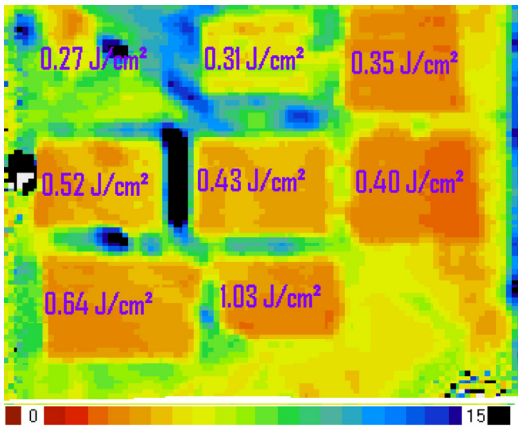

Fig. 10. Lifetime (μs) mapping of re-passivated Al_2O_3/SiN:H wafer irradiated by UV laser.

(70 nm) and a-Si:H (20 nm)/SiN:H (70 nm) stacks deposited on silicon.

The stacks are efficiently removed with the IR laser but the resulting ripple-like pattern resulting from the ablation process indicates that the silicon surface is highly affected and damaged. As a consequence, the emitter doping homogeneity can be affected and the risk of shunting is increased. The IR laser seems not well matched to this application.

We can also evoke the cost and the novelty of this kind of laser system for industry. The process speed is not adapted for long term processes and a big amount of cells to treat.

Concerning the ablation experiments done with the UV laser, the SiN:H is efficiently removed from the stacks. There are however a-Si flakes remaining on the silicon surface after ablation of the a-Si:H/SiN:H stack. On the other hand, Al_2O_3 is difficult to be removed due to its optical transparency to the UV wavelength and a rather high level of waste is present after the ablation process.

As the ablation process will be followed by Ni electroless deposition, a coming paper will show that Ni can be selectively deposited on locally laser ablated areas despite incomplete ablation of the Al_2O_3/SiN:H.

The authors would like to thank the ANR project BIFASOL ANR-11-PRGE-004 for financial support.

References

1. M. Doering, K. Meyer, A. Kaps, H.-J. Krokoszinski, H. Eschrich, in *Proceedings of 25th European Photovoltaic Solar Energy Conference/5th World Conference on Photovoltaic Energy Conversion, Valencia, Spain, 2010* (WIP, München), p. 1778
2. S.K. Chunduri, Photon Int., 158 (2010)
3. L. Tous, D.H. van Dorp, R. Russell, J. Das, M. Aleman, H. Bender, J. Meersschaut, K. Opsomer, J. Poortmans, R. Mertens, Energy Procedia **21**, 39 (2012)
4. A. Carr, *NPV Workshop, Konstanz, Germany, 2011*
5. A. Grohe, C. Harmel, A. Knorz, S.W. Glunz, R. Preu, G.P. Willeke, in *Proccedings IEEE of 4th World Conference on Photovoltaic Energy Conversion, Waikoloa, Hawai, 2006*, p. 1399
6. P. Engelhart, S. Hermann, T. Neubert, R. Grischke, N.P. Harder, R. Brendel, in *Proceedings of the 17th Workshop on Crystalline Silicon Solar Cells and Modules: Materials and Processes, Vail, Colorado, USA, 2007,* edited by B.L. Sopori (NREL, Golden, 2007), p. 57
7. S.A.G.D. Correia, J. Lossen, M. Wald, K. Neckermann, M. Bähr, in *Proceedings of 22nd European Photovoltaic Solar Energy Conference, Milano, Spain, 2007*
8. R. Preu, S.W. Glunz, S. Schafer, R. Ludemann, W. Wettling, W. Pfleging, in *Proceedings of the 16th European Photovoltaic Solar Energy Conference, Glasgow, UK, 2000* (WIP, München), p. 1181
9. P. Jaffrennou, A. Uruena, J. Das, J. Penaud, M. Moors, A. Rothschild, B. Lombardet, J. Szlufcik, in *Proceedings of 26th European Photovoltaic Solar Energy Conference, Hamburg, Germany, 2011* (WIP, München), p. 2180
10. Y. Jin, P.W. Yoon, C. Park, J. Jang, J. Kim, G. Shim, Y. Choe, J.-W. Jeong, in *Proceedings of 26th European Photovoltaic Solar Energy Conference, Hamburg, Germany, 2011* (WIP, München), p. 507
11. E.D. Palik, in *Handbook of Optical Constants of Solids*, edited by E.D. Palik (Elsevier, 1997), Vol. 1
12. A. Knorz, M. Peters, A. Grohe, C. Harmel, R. Preu, Prog. Photovolt.: Res. Appl. **17**, 127 (2009)

Cite this article as: T. Schutz-Kuchly, A. Slaoui, J. Zelgowski, A. Bahouka, M. Pawlik, J.-P. Vilcot, E. Delbos, M. Bouttemy, R. Cabal, UV and IR laser induced ablation of Al_2O_3/SiN:H and a-Si:H/SiN:H, EPJ Photovoltaics **5**, 55201 (2014).